

A&A manuscript no.  
(will be inserted by hand later)

Your thesaurus codes are:  
06(08.05.3; 08.09.2  $\eta$  Car; 08.13.2; 09.02.1; 09.10.1)

# High velocity structures in, and the X-ray emission from the LBV nebula around $\eta$ Carinae

K. Weis<sup>1,2,3\*</sup>, W.J. Duschl<sup>1,2</sup>, and D.J. Bomans<sup>4</sup>

<sup>1</sup> Institut für Theoretische Astrophysik, Tiergartenstr. 15, 69121 Heidelberg, Germany

<sup>2</sup> Max-Planck-Institut für Radioastronomie, Auf dem Hügel 69, 53121 Bonn, Germany

<sup>3</sup> University of Illinois, Department of Astronomy, 1002 W. Green Street, Urbana, IL 61801, USA

<sup>4</sup> Astronomisches Institut, Ruhr-Universität Bochum, Universitätsstr. 150, 44780 Bochum, Germany

received; accepted

**Abstract.** The Luminous Blue Variable star  $\eta$  Carinae is one of the most massive stars known. It underwent a giant eruption in 1843 in which the Homunculus nebula was created. ROSAT and ASCA data indicate the existence of a hard and a soft X-ray component which appear to be spatially distinct: a softer diffuse shell of the nebula around  $\eta$  Carinae and a harder point-like source centered on the star  $\eta$  Car. Astonishingly the morphology of the X-ray emission is very different from the optical appearance of the nebula. We present a comparative analysis of optical morphology, the kinematics, and the diffuse soft X-ray structure of the nebula around  $\eta$  Carinae. Our kinematic analysis of the nebula shows extremely high expansion velocities. We find a strong correlation between the X-ray emission and the knots in the nebula and the largest velocities, i.e. the X-ray morphology of the nebula around  $\eta$  Carinae is determined by the interaction between material streaming away from  $\eta$  Car and the ambient medium.

**Key words:** Stars: evolution – Stars: individual:  $\eta$  Carinae – Stars: mass-loss – ISM: bubbles – ISM: jets and outflows

## 1. Introduction

### 1.1. $\eta$ Carinae as a Luminous Blue Variable Star

The star  $\eta$  Carinae, embedded in the large Carina H II complex (the Carina nebula) is still one of the most unique stellar objects in our Galaxy. Known as a variable star for centuries, it brightened up to  $-1^m$  around 1843 (Herschel 1847, Innes 1903, van Genderen & Thé 1984, Viotti

*Send offprint requests to:* K. Weis, email: kweis@ita.uni-heidelberg.de

\* Visiting Astronomer, Cerro Tololo Inter-American Observatory, National Optical Astronomy Observatories, operated by the Association of Universities for Research in Astronomy, Inc., under contract with the National Science Foundation.

*Correspondence to:* K. Weis, Institut für Theoretische Astrophysik, Tiergartenstr. 15, 69121 Heidelberg, Germany

1995, Humphreys et al. 1999) and drastically decreased its brightness by more than  $7^m$  within just 20 years. While the brightness declined, discussions on the nature of this outburst started. A new hint on the origin occurred a century after the burst when nearly simultaneously Gaviola (1946, 1950) and Thackeray (1949, 1950) discovered a nebula around  $\eta$  Car. Since the appearance of the nebula on the first image was of man-like shape, Gaviola named it the *Homunculus*. Today  $\eta$  Car is classified as a *Luminous Blue Variable* (LBV).

The most massive stars (with zero-age main-sequence masses  $\geq 50 M_{\odot}$ ) start as main-sequence O stars and evolve quickly into supergiants. While they cross the Hertzsprung-Russell diagram (HRD) towards the red they seem to enter an unstable phase at an age of roughly  $3 \cdot 10^6$  years (Langer et al. 1994). This phase, the LBV phase, goes along with a very high mass loss (rates up to several  $10^{-4} M_{\odot} \text{ yr}^{-1}$ ). The strong stellar wind and possible giant eruptions where parts of the star's envelope are peeled off, often form circumstellar nebulae, the so called *LBV nebulae* (e.g., Nota et al. 1995). The LBV phase starts when the stars reach the *Humphreys-Davidson limit* (Humphreys & Davidson 1979, 1994) in the HRD. This empirical limit marks the red end of the distribution of very luminous supergiants (Humphreys 1978, 1979 and Humphreys & Davidson 1979). The most luminous, massive stars do not evolve into red supergiants but instead reverse their evolution towards the blue supergiant part in the HRD when they reach the Humphreys-Davidson limit, they turn into LBVs.

With a mass of  $M \sim 120 M_{\odot}$  and a luminosity of  $L \sim 10^{6.7} L_{\odot}$  (Humphreys & Davidson 1994, Davidson & Humphreys 1997)  $\eta$  Car is the most massive member of the LBV class known. In the light of recent discussions about  $\eta$  Car being a binary (Damineli 1996, Damineli et al. 1997, Stahl & Damineli 1998), the masses of the two components would be between 65 and  $70 M_{\odot}$  each. Both components would therefore still be among the most massive stars. The Homunculus nebula is believed to have formed during a giant eruption—the brightness increase

of 1843. Images taken with the *Hubble Space Telescope* (HST) revealed the bipolar structure of the Homunculus, consisting of two lobes each about  $8 - 9''$  in diameter (e.g., Morse et al. 1998). The original man-like shape seen around 1950 represents only the brightest emission of the bipolar lobes in the central region. Beside the two lobe structure an equatorial disk was found already through ground-based observations (Duschl et al. 1995). The deepest HST pictures (200s in the F656N-filter) show a larger amount of very complex filamentary structures like knots, arcs and strings (Weis et al. 1999) of which the sizes vary between fractions of arcseconds and several arcseconds. These structures extend much further out than the bipolar Homunculus, up to a distance of at least  $30''$  and form the outer nebula, the so-called *outer ejecta* (Weis 2000, Weis & Duschl, in prep.). The LBV nebula around  $\eta$  Carinae therefore consists of the inner bipolar Homunculus ( $\sim 17''$  in diameters) and the filamentary outer ejecta (up to  $60''$  across).

Kinematic analysis of the nebula around  $\eta$  Carinae detect astonishingly high expansion velocities, especially in the outer ejecta. In several publications radial velocities of the bipolar central and the outer nebula as high as  $1000 \text{ km s}^{-1}$  were reported (Meaburn et al. 1987, 1993, 1996, Hillier & Allen 1992, Weis et al. 1999, Weis & Duschl, in prep.). Similar velocities were derived from proper motion measurements (Walborn 1976, Walborn et al. 1978, Walborn & Blanco 1988, Currie et al. 1996).

$\eta$  Car was also found to emit in the X-ray regime, with the star being an individual point source and the dominant contributor of hard X-rays while an extended soft X-ray emission was observed from the nebula around  $\eta$  Carinae.

### 1.2. Chronology of the X-ray observations

X-ray emission of the  $\eta$  Car complex was detected by Hill (1972), observing with a proportional counter system aboard a *Terrier-Sandhawk* rocket. Observations with *Ariel 5* (Seward et al. 1976), *OSO 8* (Becker et al. 1976, Bunner 1978) and *Uhuru* (Forman et al. 1978) followed. With the launch of the *Einstein Observatory* the resolution of X-ray images was pushed down to a few arcseconds with the high resolution imager (HRI). Therefore for the first time the X-ray sources in the Carina complex could be resolved into several stars and a soft X-ray emitting diffuse component of the larger Carina H II complex (Seward et al. 1979, Seward & Chlebowski 1982).  $\eta$  Car itself was just one extended source. The extended soft X-rays compared to the optical data, showed their origin in the nebula around  $\eta$  Carinae (Seward et al. 1979). The authors excluded a supernova as formation mechanism for the X-radiation and proposed that they formed through a blast wave from the  $\eta$  Car outburst. The Einstein observations also showed that there was a hard X-ray source located somewhere in the Homunculus.

The first detailed analysis of the X-rays from  $\eta$  Car and its nebula, with a longer Einstein observation, as well as a comparison of the X-ray with the optical image was done in 1984 (Chlebowski et al.). This first overlay already identified the most intense X-ray emission with structures in the outer ejecta, namely the *S condensation*, the *W arc* and the *E condensation* (for the notation of the knots see Walborn 1976). The observed X-rays result mainly from the outer shell of  $\eta$  Car and are soft in nature. In addition the harder central source (not resolved with the Einstein *Imaging Proportional Counter*, IPC) was tentatively identified with the star  $\eta$  Car itself. The measurements of the *Ginga* satellite sensitive to hard X-rays ( $2 - 37 \text{ keV}$ ) prove the existence of a harder source with a temperature of  $4.1 \text{ keV}$  in the Carina nebula (Koyama et al. 1990).

ROSAT improved the resolution and sensitivity in the soft X-ray band even further.  $\eta$  Car was observed with ROSAT in both the *Position Sensitive Proportional Counter* (PSPC; spatial resolution  $\sim 25''$ ) and in the *High Resolution Imager* (HRI; spatial resolution  $\sim 5''$ ). Several discussions on the ROSAT data prove now the existence of a harder and softer X-ray component of  $\eta$  Car and its nebula (c.f., Corcoran et al. 1994, 1995, 1996, 1997), which are spatially distinct: a softer diffuse shell of the nebula and a harder point-like source centered on  $\eta$  Car. In addition it was found that the hard X-ray source shows variability and a pointlike character (Corcoran et al. 1995).

Analogous results were achieved with the *Advanced Satellite for Cosmology and Astrophysics* (ASCA; Tsuboi et al. 1997, Corcoran et al. 1998). Due to the good spectral resolution of ASCA it was also possible to conclude that the 'X-ray variability does not involve measureable changes to the spectral shape of the emission' (Corcoran et al. 1998).

### 1.3. Structure of the paper

In this paper, we present the results of a comparative study of images from the HST, high-resolution long-slit echelle spectra and X-ray data. We will give an interpretation of the origin of the X-rays and explain the different morphological appearance of the optical and the X-ray emission of the nebula around  $\eta$  Car.

## 2. Observation and data reduction

### 2.1. X-ray data

For the analysis of the X-ray emission from the LBV nebula around  $\eta$  Car we made use of archived data from the *Röntgensatellit* (ROSAT). The ROSAT satellite was sensitive to X-ray emission between  $0.1$  and  $2.4 \text{ keV}$ . Images of the  $\eta$  Car region were taken with the PSPC as well as the HRI. We used mainly the high spatial resolution data taken with the HRI (first HRI images published by Corcoran et al. 1996) since the small X-ray nebula around  $\eta$

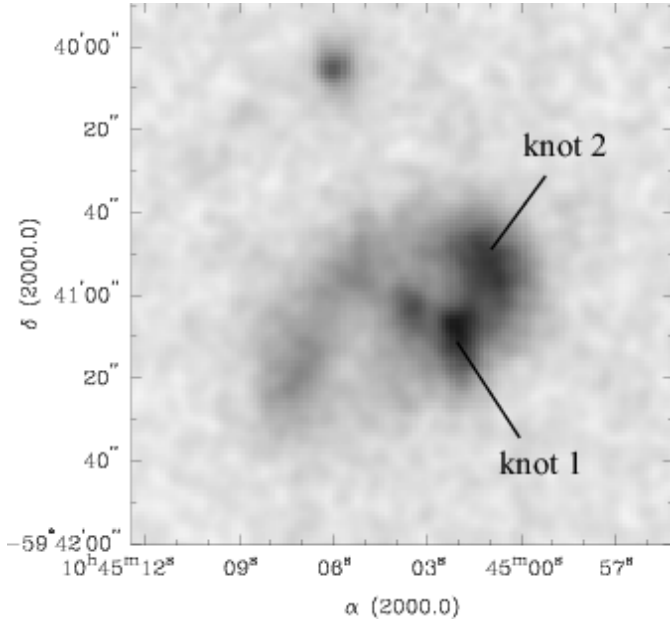


**Fig. 1.** ROSAT HRI image of the full usable integration time of  $\eta$  Car and its nebula. The field of view is about  $2' \times 2'$ . The image was smoothed with a Gaussian filter to an effective resolution of  $5''.5$ . The marked knots 1 and 2 are defined in the text.

Car is barely resolved in the PSPC data (Corcoran et al. 1994). All exposures available for the Carina region (see Tab. 1) were retrieved from the *Max-Planck-Institut für Extraterrestrische Physik* (MPE) ROSAT data center.

Data reduction was performed with IRAF<sup>1</sup>/PROS<sup>2</sup>. Three individual HRI pointings were long enough ( $> 5$  ksec) to contain significant information about the diffuse emission around  $\eta$  Car. First we screened the data for periods with excessively high background. Since highest possible spatial resolution was essential for our work, as next step we checked for errors in the aspect solution, using methods similar to the methods described in Harris et al. (1998). To ensure a stable pointing, we excluded observing time with less than three guide stars present. The total usable integration time adds up to 95 ksec. Next we produced images of the individual observational intervals (OBIs) and re-centered these individual images. Shifts were generally small but not negligible, between  $1''$  and  $4''$ . The count rates in the brightest X-ray point source, which could be used for positional shifts, was unfortunately too low to split the OBIs even more into individual phase bins to investigate residual effects of the spacecraft wobble. We chose a blocking factor of 2, resulting

<sup>1</sup> IRAF is distributed by the National Optical Astronomy Observatories which is operated by AURA, Inc. under cooperative agreement with the NSF.

<sup>2</sup> PROS is developed, distributed, and maintained by the Smithsonian Astrophysical Observatory, under partial support from NASA contracts NAS5-30934 and NAS8-30751.

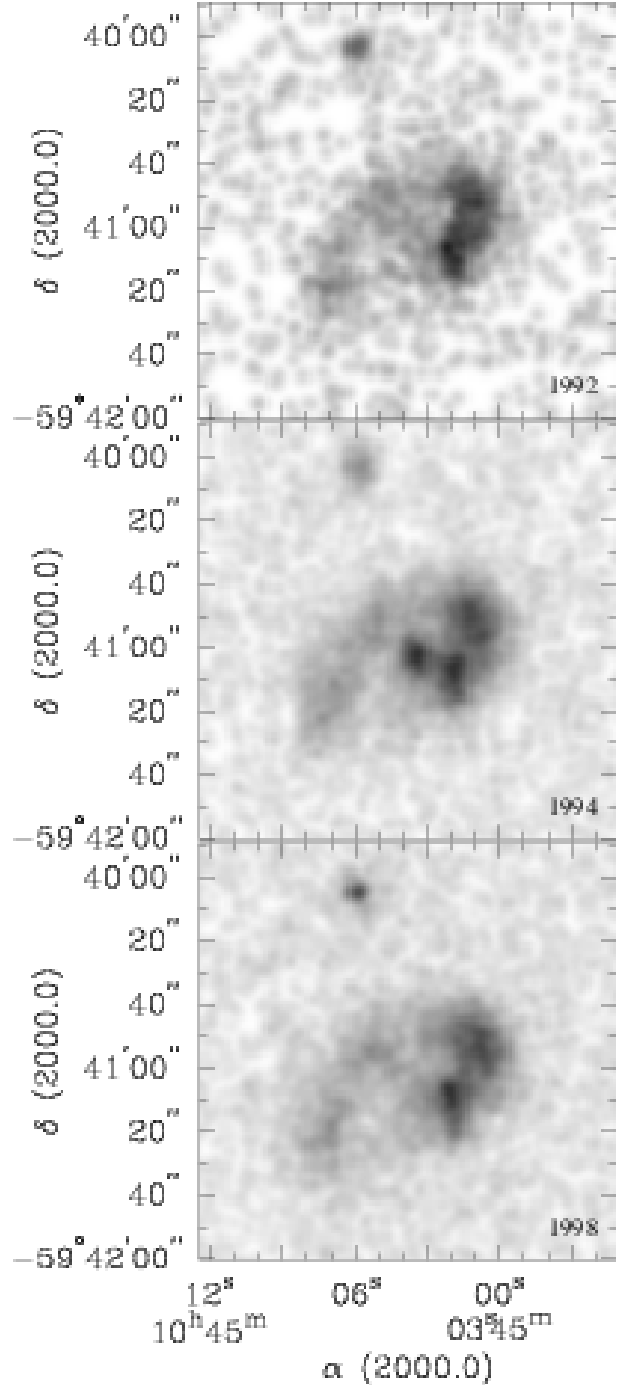


**Fig. 2.** HRI images of the  $\eta$  Carinae nebula during the three observing intervals which are long enough to show the X-ray nebula (see table 1). The three panels show the images generated from the 1992 (upper panel), 1994 (middle panel) 1998 (lower panel) data sets.

in  $1''$  per pixel and smoothed the images slightly with a  $\sigma = 1.5$  pixel Gauss filter. We updated the coordinates using the five X-ray point sources coinciding with the stars HD 93205, HDE303308, CD- $59^{\circ}2635$ , CD- $59^{\circ}2636$ , and CD- $59^{\circ}2641$  in the Carina nebula. The coordinates of the

**Table 1.** ROSAT HRI Observations of  $\eta$  Car; the column offset gives the offset of the image center from  $\eta$  Carinae.

pointing	Obs. interval	P.I.	exposure time [s]	offset [']	comment
rh150037n00	900727-900729	Puls	3351	7.135	
rh900385n00	920731-920802	Schmitt	11527	0.31	source off
rh900385a01	940106-940106	Schmitt	522	0.31	
rh900385a02	940721-940729	Schmitt	40555	0.31	source on
rh900644n00	960813-960813	Corcoran	1720	0.31	
rh202331n00	971223-980210	Corcoran	47095	0.31	source off

stars were measured on a Digital Sky Survey (DSS) image using the IRAF/GASP package. The resulting positional accuracy of the X-ray images is of the order of  $0''.5$  relative to these stars. From the new photon file we produced three images of the three observations in 1992, 1994 and 1998, according to the central source's high or low state. In addition a total flux image (Fig. 1) was made, combining all observations regardless of the state of the central source. The images are shown in Fig. 2, in which the upper panel gives the 1992 (low state), the middle one the 1994 (high state), and the lower one the 1998 (low state) data.

## 2.2. Optical Imaging

To compare the X-ray data with an optical image of the nebula around  $\eta$  Car, data were taken from the HST Archive at the *Canadian Astronomy Data Centre* (CADC). Images of the *Wide Field Planetary Camera 2* (WFPC2) with the F656N ( $H_\alpha$ ) filter were retrieved<sup>3</sup>. Their reduction, combination and cosmic-ray cleaning followed the standard procedures recommended for WFPC2 data in IRAF. The exposure times ranged from 0.11 to 200 seconds. The reduced and mosaiced F656N image was used for an overlay with the total integration time X-ray image (Fig. 3) and the comparison between the X-ray and the optical emission. In addition it was used to identify several knots in the outer nebula, for which we took kinematic data.

## 2.3. Long-slit echelle spectroscopy

Kinematic information was obtained using long-slit echelle spectroscopy. The data were taken by one of us (KW) with the 4m Blanco telescope at the *Cerro Tololo Inter-American Observatory* (CTIO) in the long-slit mode. Wavelength selection was achieved by inserting a post-slit  $H_\alpha$  filter ( $6563/75 \text{ \AA}$ ) and replacing the cross-disperser by a flat mirror. We choose the  $79 \text{ lmm}^{-1}$  echelle grating, a slit-width of  $250 \mu\text{m}$  ( $\cong 1''.64$ ), which leads to an instrumental FWHM at the  $H_\alpha$  line of about  $14 \text{ km s}^{-1}$ . The data were recorded with the long focus red camera and the Tek2K4 CCD ( $2048 \times 2048$ ). Here the pixel size was  $0.08 \text{ \AA pixel}^{-1}$  along the dispersion, and  $0''.26 \text{ pixel}^{-1}$  on

<sup>3</sup> F656N – program number: 5239; P.I.: J.A. Westphal; dataset names: U2DH0101T ... U2DH0106T

the spatial axis. Vignetting limited the slit length to  $\sim 4'$ . During all observations the weather was not photometric and the seeing was between  $1''.5 - 2''$ . Thorium-Argon comparison lamp frames were taken for wavelength calibration and geometric distortion correction.

The whole dataset contains 31 slit positions, of which the central 6 positions around  $\eta$  Car could not be used, because strong straylight from the dusty Homunculus and extended ghost images did not allow us to extract reliable information from the spectra. The individual observations were offset by  $2''$  each from an offset star rather than  $\eta$  Car itself, since the position of  $\eta$  Car is confused by strong emission of the Homunculus. The orientation and position of the slits are indicated in Fig. 4. With the mapping a field of about  $60'' \times 60''$  around  $\eta$  Car was covered. In Fig. 5 we give three example spectra with individual knots marked by numbers. The spectra cover a range of  $80 \text{ \AA}$  centered on  $H_\alpha$ , thus they include also the [N II] lines at  $6548$  and  $6583 \text{ \AA}$ . The spatial extent is  $1'.5$ . Usually the features are more prominent in the [N II] lines than in  $H_\alpha$  due to the CNO cycle processed material in the nebula.

Figure 3 shows the overlay of the X-ray emission in contours onto the HST image, velocities (in  $\text{km s}^{-1}$ ) represent the kinematics in the lower panel. Clearly a lack of data can be seen in the center, where the information of the 6 slit positions is missing. A rotation of the slit placed the spectra to a position angle of  $\text{PA} = 132^\circ$ , i.e. along the major axis of the bipolar nebula. A more detailed description of the observations and the spectra will be published separately (Weis & Duschl 2000, in preparation).

## 3. X-rays from the $\eta$ Car region

### 3.1. The morphology of the $\eta$ Car X-ray nebula from ROSAT HRI data

In this paper we concentrate on the X-ray emission from the  $\eta$  Car LBV nebula. The X-ray image with the highest spatial resolution, the ROSAT HRI image, can be seen in Fig. 1.

The X-ray nebula around  $\eta$  Car extends much further out from  $\eta$  Car than the two lobes of the Homunculus (Fig. 3), the *S Ridge* and the *N Condensation* (for notations see Walborn 1976). Instead of the bipolarity of the optical structure, the X-ray nebula consists of a hook-shaped diffuse emission region, roughly encircling the cen-

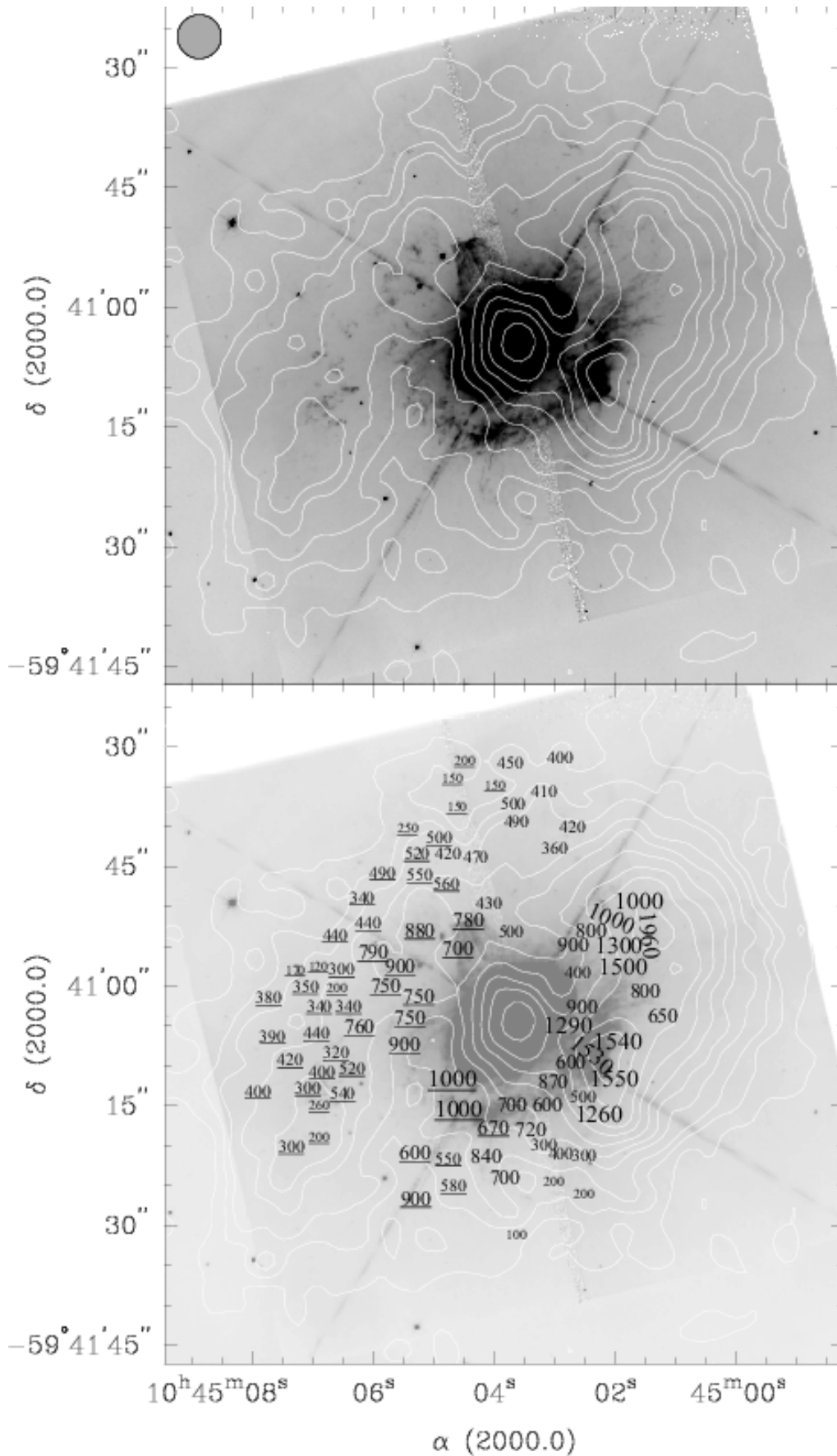


**Fig. 3.** Overlay of the X-ray emission (contour lines) and the HST image (grey scales): In the upper left corner of the top panel the ROSAT HRI resolution ( $5'' \times 5''$ ) is indicated. The lower panel shows the same overlay (with decreased grey scale intensity), with the measured radial velocities (in  $\text{km s}^{-1}$ ) placed at their respective positions. Underlined numbers indicate negative velocities. The sizes of the characters increase with increasing absolute velocities (see text). Due to their low surface brightness, occasionally the clumps and knots for which velocities are given, can be identified on the HST image but do not show up clearly in this print.

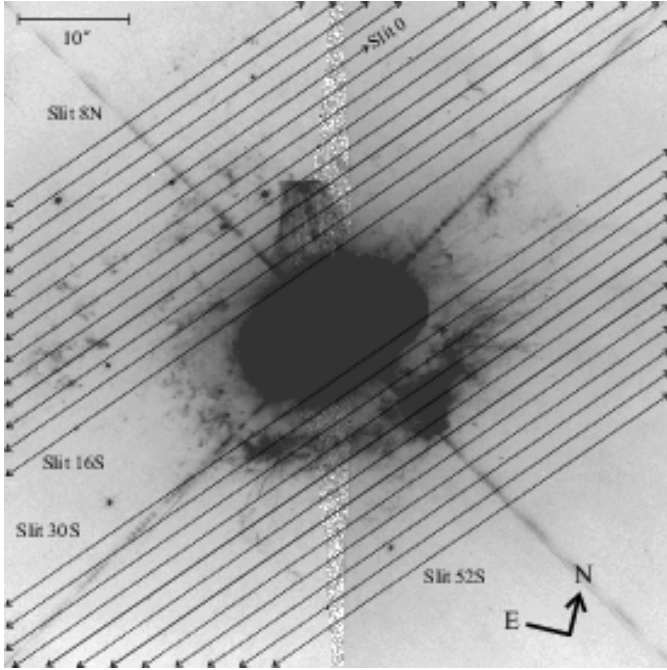


**Fig. 4.** This figure marks the position of the slits of the echelle spectra with dashed and solid lines. The image shows a  $60'' \times 60''$  section of the unrotated F656N HST image from  $\eta$  Carinae. A north-east vector indicates the celestial orientation of the image. To avoid confusion, only some necessary slit names are indicated. Slits drawn with solid rather than dashed lines represent the positions of the slits for which echellograms are given in Fig. 5

tral point-like source. About one-third (position angles  $PA \approx 210 - 330^\circ$ ) of the loop is of high X-ray surface brightness. At about  $PA \approx 330^\circ$  the surface brightness abruptly drops by a factor of three and stays at this level for the range  $PA \approx 330 - 130^\circ$ ; the remainder is at an even weaker, barely detectable surface brightness.

Several local maxima of the X-ray surface brightness are visible in the X-ray nebula (Fig. 1 and 3). In the south-west the brightest maximum is located ( $\alpha \approx 10^{\text{h}}45^{\text{m}}2^{\text{s}}.0$ ,  $\delta \approx -59^\circ41'08''$ ). In the following we will refer to it as *knot 1*. It coincides roughly with the *S condensation*. The X-ray maximum is approximately triangular, with a corner pointing into the direction of the central source. A fainter extension follows to the south. A second maximum (at  $\alpha \approx 10^{\text{h}}45^{\text{m}}1^{\text{s}}.4$ ,  $\delta \approx -59^\circ40'53''$ ) peaks to the north-west of  $\eta$  Car (*knot 2*), in a part of the nebula where no bright optical counterpart but only low surface brightness clumps and knots can be identified. Knot 2 in the X-ray image seems to consist of two or three subentities.

Two local maxima in surface brightness are embedded in the low surface brightness part of the X-ray nebula north and east of  $\eta$  Car (at  $\alpha \approx 10^{\text{h}}45^{\text{m}}4^{\text{s}}.5$ ;  $\delta \approx -59^\circ41'23''$  and at  $\alpha \approx 10^{\text{h}}45^{\text{m}}5^{\text{s}}.5$ ,  $\delta \approx -59^\circ40'58''$ ). The two maxima are less peaked and more extended than the

maxima in the high surface brightness part of the  $\eta$  Car X-ray nebula.

A closer look at the central point source indicates that it is elongated ( $PA \approx 30^\circ$ ), while the other point sources in the field are round. This excludes that the shape of the central source is produced by residual uncertainties of OBI centering or wobble. Deviation of the measured point spread function of the HRI from the theoretical expected circular symmetric shape occur (“meaty sources”) and are independent of the wobble, but should be present in all sources with small off-axis angles in a given exposure (Briel et al. 1994). A radial plot of the central point source is shown in Fig. 6 in comparison with the radial brightness profiles of the nearest isolated star in the  $\eta$  Car X-ray image (HD303308), and the standard point source HZ43 (extracted from calibration observations from the ROSAT archive). While the correction for the diffuse extended emission visible in the radial profile of the central X-ray source of  $\eta$  Car is a matter of concern for this comparison, the slope of the fall-off is shallower than the slope of the comparison point sources. The elongation of the central source should therefore be intrinsic and indicates a second extended emission component in addition to  $\eta$  Car itself. The orientation is consistent with it being part of the equatorial disk, as defined by Duschl et al. (1995). A first inspection of the  $\eta$  Car data from the CHANDRA satellite seem to support our observation, showing a point source and an elongated halo, but these data definitely need a more careful analysis.

When comparing the X-ray images produced from the three data sets with sufficiently long exposure time (see Fig. 2) some differences can be discerned in the nebula itself between the older low state image (1992 data set, Fig. 2 upper panel) and the high state image (1994 data set, Fig. 2 middle panel), despite the lower signal-to-noise ratio of the image at low-state. The shape of knot 1 appears different, with the brightest spot being more distant from  $\eta$  Car in the high state image which was taken at a later date. The morphology of knot 2 appears different, too, but interpretation is severely hampered by low count-rate in the low-state image. The effective spatial resolution is the same in both images, the more fuzzy looking appearance of HDE303308 (north of  $\eta$  Car) is an effect of the different brightness cuts of the images. The faint nebula south-east of the central source seems to be connected with diffuse emission visible at the position of the point source (at low state).

The newer, 1998, low state image (see Fig. 2, lower panel) is better suited for such a comparison since the signal-to-noise ratio (S/N) is comparable to the high state image. Ratio images like Fig. 7 seem to imply that in addition to some fluctuations of surface brightness, the region of knot 2 brightened from 1992 to 1998. This effect may have created the impression of expansion of the nebula as proposed by Corcoran (priv. comm., and <http://lheawww.gsfc.nasa.gov/users/corcoran/eta.car/>

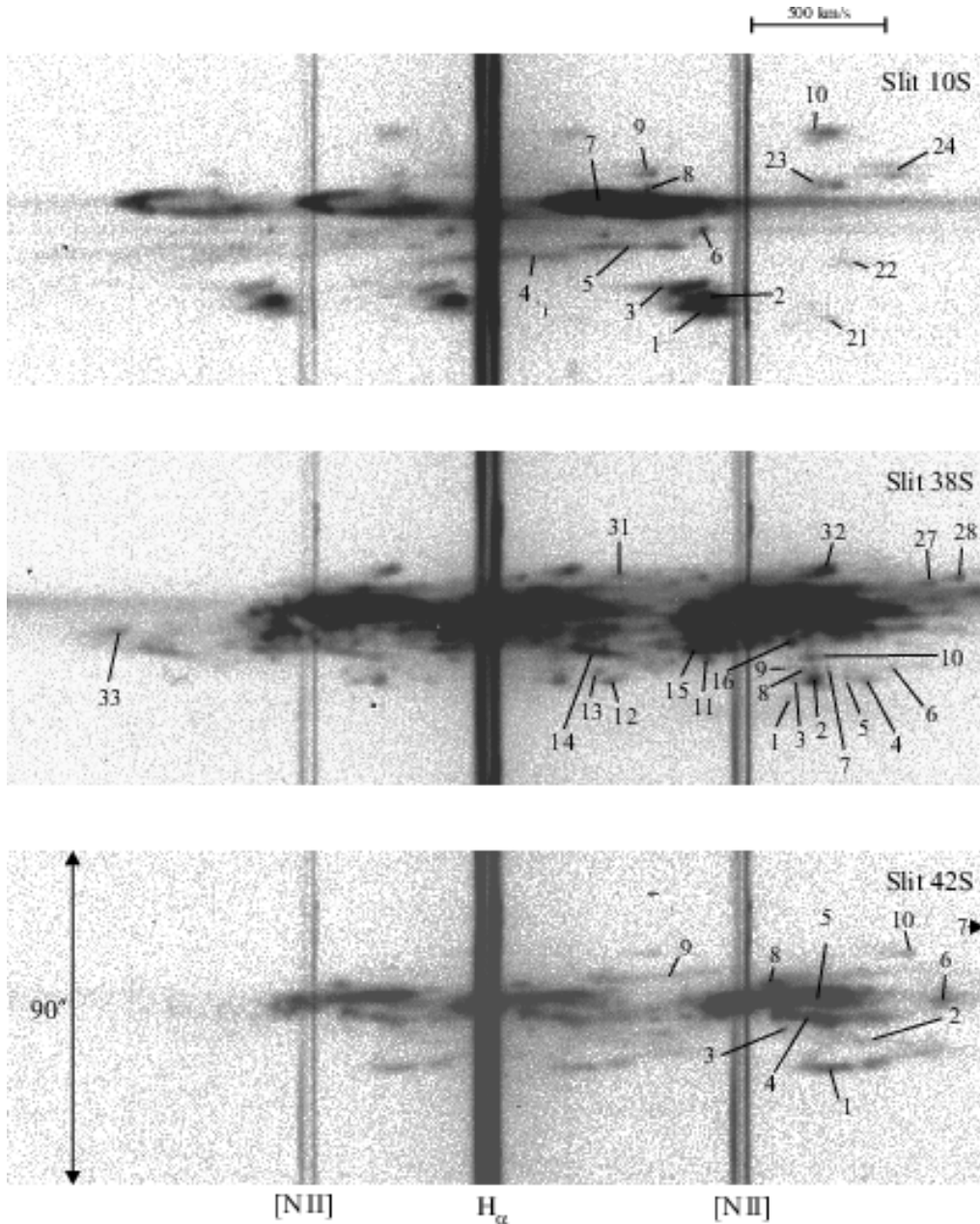


**Fig. 5.** Three typical Echellograms of our mapping: They cover a wavelength range of  $80 \text{ \AA}$  each. Continuous split lines indicate the expansion of the gas in the background nebula in the vicinity of  $\eta$  Car. Numerous knots and clumps are identified with a broad range of velocities. Numbers mark individual knots.

eta\_car.html#HRI). The change in knot 1 seems not to be confirmed by the 1998 data. The faint emission at the position of the central source seems to be present in both the 1992 and 1998 data sets.

This global expansion hypothesis by Corcoran reveals one major problem, it predicts extremely high ( $\sim 10\,000 \text{ km s}^{-1}$ ) expansion velocities, which are not found up to now. We tested several signal to noise cuts and noted that in regions of low but still acceptable S/N some brightening occurs. Since this effect is also visible at the rim of the point source HD303308 (the star north of  $\eta$  Car), this may imply this rim brightening in the ratio images is an artifact of low count rate and subsequent image processing.

Still there is an effect visible in Fig. 7: as stated above, the region of knot 2 seems to have brightened somewhat

(factor of about 1.6) in the 1998 data set compared to the 1994 data set (and to lower confidence level compared to the 1992 data set). Contrary to all the other differences between the images, which are below the formal ‘beam-size’ of the HRI and therefore not significant, this effect is spatially extended and therefore, in all likelihood, real.

#### 4. Comparison of the X-ray morphology, the kinematics and the HST narrow band image

As described in Sect. 3.1, the morphology of the X-ray nebula and the optical appearance of the nebula around  $\eta$  Carinae are remarkably different. Except for  $\eta$  Car itself and the South Ridge, there seems to be no direct cor-

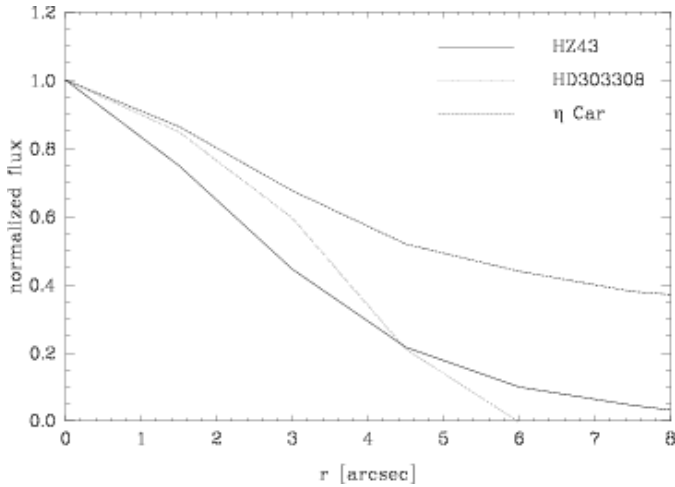


**Fig. 6.** Radial X-ray brightness profiles of the central source of  $\eta$  Car and two comparison point sources, the most nearby X-ray bright star in the  $\eta$  Car field (HD303308) and the ROSAT standard point source HZ43. Note that the slope of the  $\eta$  Car profile is much shallower than the slope of the two point sources.

relation between the emission line image and the X-ray distribution (Fig. 3, top panel).

Our echelle spectra show a great deal of fine structure which mainly results from numerous individual knots distributed all over the observed region. In Fig. 5 we give examples for three different slit positions (Slit 10S is located 10'' south of our offset star, star #60 in Thé et al. 1980, at a position angle of 132°, Slits 38S and 42S are at 38'' and 42'' south, respectively, at the same angle; for slit positions see Fig. 4). We have marked a number of kinematically coherent structures. This was carried out for all spectra; we then identified these structures with knots and clumps on the HST image. Due to the much higher spatial resolution of the HST in comparison with our spectra, occasionally we found that structures that appear coherent in the spectra consist of several smaller morphological entities.

In the lower panel of Fig. 3 we give the maximum radial velocities for individual knots and clumps. If in a small area there are several knots with similar maximum radial velocities, we give only the highest value of the entire ensemble. To keep the crowding in the figure as small as possible, negative velocities are underlined rather than marked by a minus sign. In order to give the reader an easy overview, we have binned the radial velocity ( $v_{\text{rad}}$ ) markings such that we used four different font sizes, the smallest one for  $|v_{\text{rad}}| \leq 300 \text{ km s}^{-1}$  and ever increasing ones for  $300 \text{ km s}^{-1} < |v_{\text{rad}}| \leq 600 \text{ km s}^{-1}$ ,  $600 \text{ km s}^{-1} < |v_{\text{rad}}| \leq 1000 \text{ km s}^{-1}$ , and  $1000 \text{ km s}^{-1} < |v_{\text{rad}}|$ .

A combination of the three pieces of information, morphology of the HST image, radial velocities of the clumps and knots, and morphology of the X-ray image clearly

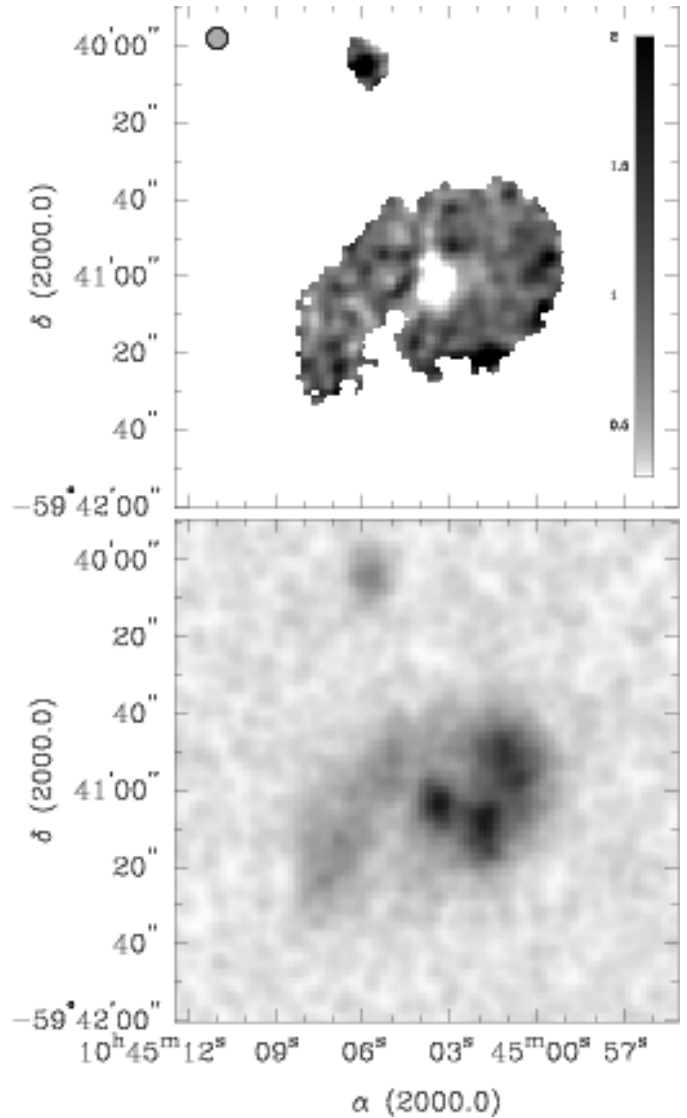


**Fig. 7.** The upper panel shows the ratio map between the 1994 and 1998 HRI data sets. Dark regions are brighter in the 1998 data. The lower panel shows for comparison the image of the X-ray nebula. The effective resolution of both images is plotted as filled circle in the upper panel.

shows a good correlation between the X-ray intensity and the absolute values of the radial velocity (lower panel of Fig. 3). The most intense regions in the X-ray image are those where one finds the knots with the highest velocities. This, however, is usually not a region where one finds strong emission in the optical (HST image). We refer the reader to the above discussed positions, for instance, where maxima of the absolute value of the radial velocity and of the X-ray intensity coincide.

There is also a correlation between the lack of X-radiation and the lack of material in the nebula around  $\eta$  Car. A comparison of Figs. 1 and 3 (lower panel) shows that X-ray emission is missing south of  $\eta$  Car (in the area

of  $\alpha \approx 10^{\text{h}}45^{\text{m}}05^{\text{s}}$ ,  $\delta \approx -59^{\circ}42'20''$ ), a region where there are also less knots and clumps.

However, when comparing X-ray intensities and radial velocity maxima, one has to keep in mind that

- radial velocities are good and bad tracers of the kinematics of the material at the same time: While they give a lower limit of the true three dimensional velocity of the material, they suffer from the projection effect onto the line of sight. For motions almost tangential to the celestial sphere, a thus determined lower limit of the full velocity is no longer very meaningful. Unfortunately outside of the Homunculus, in the outer ejecta only very few proper motion measurements are available (Walborn et al. 1978, Walborn & Blanco 1988). For these measurements we find that the radial velocities are in almost all cases comparable to or larger than the tangential velocities, i.e., good tracers of the full velocity field.
- the highest velocities are not necessarily where the shocks run into the densest clumps, which would be the dominant producer of X-rays.
- due to the lack of observable material—be it due to a true local void, be it due to a too low brightness—the sampling of the distribution of the radial velocities necessarily must be less complete than that of the X-ray surface brightness.

The global distribution of the radial velocity maxima follows the same orientation as the Homunculus, namely positive radial velocities in the north-west and negative ones in the south-east. We will discuss this in detail in a later paper (Weis 2000, Weis & Duschl, in prep.)

## 5. Discussion

Having established the spatial correlation between the peaks in X-ray surface brightness of the nebula around  $\eta$  Car with regions of especially high radial velocity of the warm ionized medium, we propose the following model for the X-ray surface brightness distribution: material streaming away from  $\eta$  Car—presumably having originated in the giant eruption of 1843—interacts with the ambient medium. This occurs with the large relative velocities as indicated by the radial velocity measurements. The X-ray intensity is governed by the resulting shock velocities and the densities. Due to the bandwidth of ROSAT and in particular due to the high foreground H I column density ( $\log N_{\text{H}} \approx 21.3$ , e.g., Savage et al. 1977) only gas heated by shocks with velocities  $\geq 300 \text{ km s}^{-1}$  is observable. This implies that only high velocity shocked gas is traced.

Knots 1 and 2 are the regions of highest X-ray surface brightness in the X-ray nebula and coincide with regions with radial velocities of about  $1500$  and  $1900 \text{ km s}^{-1}$ , respectively. These high velocities correspond to lower limits of the post-shock plasma temperatures ( $T_{\text{ps}}$ ) of  $3 \cdot 10^7$  and  $5 \cdot 10^7 \text{ K}$ , with  $T_{\text{ps}} = V^2(3\mu/16k)$  (see McKee 1987;  $V$ :

radial velocity taken as representative for the shock velocity;  $\mu$ : mean mass per particle). We assumed for these estimates a normal He/H ratio of 0.1 leading to  $\mu = 0.61$  for a fully ionized gas. Using a higher He/H ratio, as one would expect for the ejecta of  $\eta$  Car (increased He and N, decreased C and O as a consequence of the CNO cycle), the resulting post-shock temperatures would be even higher (e.g. by a factor of 1.5 for He/H= 0.33). These estimates unfortunately do not define directly the overall intensity of the X-ray emission. Such high temperature gas has to be present, but it needs not to be associated with high surface brightness. To get a better handle on the plasma temperature dominating the X-ray flux, we can use the velocity structure of the X-ray knots: The echelle spectra show that clumps in this region with high surface brightness move predominantly with velocities of around  $700 \text{ km s}^{-1}$ . If the  $\text{H}\alpha$  and  $[\text{N II}]$  surface brightness is a reliable tracer of the average gas density, we can predict that the X-ray plasma has a temperature of about  $8 \cdot 10^6 \text{ K}$ , only somewhat higher than the temperature of the soft component observed with ASCA (Corcoran et al. 1998).

Over most of the area of the nebula the typical velocities are smaller and about  $400 \text{ km s}^{-1}$  to  $600 \text{ km s}^{-1}$ , implying a lower limit for the plasma temperature of  $2 - 5 \cdot 10^6 \text{ K}$ .

ASCA spectra of the  $\eta$  Car X-ray nebula (Corcoran et al. 1998) show that the emitting plasma can be well fitted with a two component model, having plasma temperatures of  $3.2 \cdot 10^6$  and  $6.3 \cdot 10^7 \text{ K}$ . The authors attributed the low temperature component to the extended X-ray nebula and the hard component to the central source ( $\eta$  Car) itself. This idea is supported by the limited information of the structure of the X-ray nebula present in the PSPC data (Corcoran et al. 1995) for the eastern part of the nebula. Interestingly, the temperature from the integrated ASCA spectra fits well with the post-shock temperatures derived above. But there is an additional piece of evidence concerning the properties of the X-ray nebula: during new ASCA observation the central source was in low state. Corcoran et al. (2000) found that while the plasma temperatures of both the hard and soft spectral component stays the same within the errors, the absorbing H I column densities of the hard spectral component decreases together with the flux of the hard component. Using these new ASCA data together with measurements at high state, about 3% to 6% of the hard flux is still present, when the central source is in low state (Corcoran et al. 2000). The location of this hard emission is uncertain due to the large ASCA PSF size, but recent CHANDRA data may support that the emission is extended (see also Corcoran et al. 2000), and as already suggested in Section 3.1. The lower limits of the post-shock temperature implied from the radial velocities fit perfectly to the measured temperature of the soft X-ray component. Even more the presence of the very high velocity gas implies

that the extended nebula at least contributes partly to the flux in the hard component.

The most distant regions of the nebula around  $\eta$  Carinae show expansion velocities of only  $200 \text{ km s}^{-1}$  which would imply a post-shock temperature of  $5 \cdot 10^5 \text{ K}$ , too low to be detected with the ROSAT HRI. Therefore, the sharp boundary of the X-ray nebula in the north and east can be understood as an effect of the motion of the nebula, too. In the south-west region lower surface brightness wings from knot 1 and 2 extend into regions where no high velocity optical emission is detected. This gas might be missing because its optical emission is very faint and below the detection limit of both the HST images and our echelle data. If that is not the case some streaming of hot gas is needed to explain the observations, instead of in situ creation of the hot gas due to fast shocks passing through relatively dense gas.

A derivation of electron densities of the ambient medium from the F656N filter HST image is not possible, as highly shifted [N II] emission contaminates the  $H_\alpha$  band. While it is tempting to derive electron densities and the thermal energy content (e.g. Chu & MacLow 1990) of the knots 1 and 2, we decided against this exercise, since the correction factors from the ROSAT HRI fluxes in the 0.1 to 2.4 keV band to the approximate temperatures of the X-ray gas in the knots of at least  $3 \cdot 10^7 \text{ K}$  would be too large. If we assume that the typical temperature of the knots is defined by the velocity of the majority of the structures in the knot 1 and 2 (about  $700 \text{ km s}^{-1}$ ), rms electron densities could be derived. But still, due to the complexity of the shape of the X-ray emitting knots and the fact that they consist of multitudes of different clumps moving at different velocities, the values would be almost meaningless for the physical state of the emitting gas. Additionally, the temperature of the hot gas is derived for thermal equilibrium (using Raymond-Smith plasma models), while the topology of the emitting region and the small time scales appropriate for  $\eta$  Carinae (of the order of 100 years!) implies strongly non-equilibrium conditions. High spatial resolution and high signal to noise spectra as obtainable with the CHANDRA satellite may be able to probe this and derive meaningful physical parameters for the X-ray emitting plasma in the  $\eta$  Carinae nebula. Still, it is interesting to note, that the X-ray surface brightness in the ROSAT energy band of knot 1 and 2 are comparable or even larger than that of the central source itself.

If the contribution of the nebula to the hard X-ray emission of the nebula around  $\eta$  Car is relatively small, as implied by the ROSAT PSPC results (Corcoran et al. 1995) and the new CHANDRA data (Seward et al. 2001), we are left with a problem: why are pronounced bright spots of the relatively soft X-ray emission, namely knot 1 and 2, at the exact position of the fastest moving structures seen in our echelle spectra? The X-ray emission does not correlate well with the surface brightness of the ionized gas or even the surface brightness or number density

of the knots moving faster than  $300 \text{ km s}^{-1}$ , which are able to produce observable X-ray emission of the  $\eta$  Carinae nebula. If the X-ray emission at these knots is not dominated by hard X-ray emission produced by the very fast shocks implied by our velocity measurements, as the early release CHANDRA data imply, we need another process to explain this tight correlation.

One way out could be the following: If for the gas the time after the passage of the fast shock is too short to reach thermal equilibrium, the kinetic temperature of the gas is high, while the adaption of ionization state runs ahead. Such non-equilibrium effects were discussed by e.g. Schmutzler & Tscharnuter (1993). Without knowledge of the exact ionization history we can only check the feasibility of this idea using time-scales. We use here Nitrogen as a trace element, since the normally dominant coolant Oxygen is strongly suppressed in the ejecta nebula of  $\eta$  Car due to the CNO cycle (Davidson et al. 1982, Dufour et al. 1997). At  $5 \cdot 10^7 \text{ K}$  the dominant ion of Nitrogen is N VI (Sutherland & Dopita 1993). Using the recombination coefficient calculated with the tabulations of Shull & van Steenberg (1982) and a typical density in the outer ejecta (more precise the S ridge) of at least  $n_e \sim 12000 \text{ cm}^{-3}$  (Dufour et al. 1997) the recombination time is  $\sim 50$  yrs. Using the cooling coefficients tabulated by Sutherland & Dopita (1993) and the same density the cooling time of this plasma is 1400 yrs. We would therefore observe a plasma which appears colder when measured from its ionization state, than it is according to its internal state. The net effect is that an analysis with an equilibrium plasma code would derive a too low temperature, since the line emission and therefore the ionization conditions dominate the spectrum. This may be the case for the knots 1 and 2 and could present the solution for the otherwise strange correlation of the highest velocities with peaks of relatively low temperature X-ray plasma traced by the ROSAT HRI images. Most other regions of the nebula would be near equilibrium conditions as indicated by the close match of the X-ray temperature and the post-shock temperatures derived from our high resolution echelle spectra.

Again, to test this idea, high spatial and spectral resolution X-ray spectra with good signal to noise are needed, which may be provided by CHANDRA observations.

## 6. Summary

A comparison of the morphological appearance of the  $\eta$  Car nebula in the optical (HST F656N filter) and the X-ray (ROSAT HRI) wavelengths ranges shows remarkable differences. Adding as a third piece of information the kinematics of the material, one finds that there is a strong correlation between the largest absolute values of the radial velocities of knots and clumps and the areas of the highest X-ray surface brightnesses. This offers as an explanation that the X-radiation as traced by the HRI images comes predominantly from regions where material stream-

ing away from  $\eta$  Car interacts with the ambient medium and gives rise to shock fronts. The observed velocities allow us to derive a post-shock temperature. The resulting value is in good agreement with temperatures derived from ASCA spectra, but is contradicted to the limited spatial information provided by the ROSAT PSPC. While some contribution of the nebula the hard emission is still possible, the problem is to reconcile the strong correlation of the region of highest velocity (not surface brightness) ionized gas with the strongest X-ray peaks. With the current data non-equilibrium ionization appears the only way out, but better spectra are highly needed to test the idea. In summary, one can say that while the morphology of the optical and the X-ray images are rather different, the underlying physical process, i.e., the interaction between the material streaming away from  $\eta$  Car and the ambient medium yields the clue to the relation between the images in the two wavelengths regimes.

*Acknowledgements.* KW is grateful to Prof. You-Hua Chu for motivation and discussions on the subject of this paper. DJB thanks the ITA director Prof. Dr. W.M. Tscharnuter and the ITA staff for their great hospitality during the several visits while working on this paper. The authors thank the referee, Dr. M. Corcoran, for many comments and suggestions which helped to improve the paper considerably. The data reduction and analysis was in part carried out on a workstation provided by the *Alfried Krupp von Bohlen und Halbach Stiftung*. Guest User, Canadian Astronomy Data Centre, operated by the Herzberg Institute of Astrophysics, National Research Council of Canada. Data retrieved from the ROSAT archive at MPE Garching.

## References

- Becker R.H., Boldt E.A., Holt S.S., et al., 1976, ApJ 209, L65  
 Briel U.G., Aschenbach B., Hasinger G., et al., 1994, The ROSAT Users' Handbook, MPE Garching  
 Bunner A.N., 1978, ApJ 220, 261  
 Chlebowski T., Seward F.D., Swank J., Szymkowiak A., 1984, ApJ 281, 665  
 Chu Y.-H., Mac Low M.-M., 1990, ApJ 365, 510  
 Corcoran M.F., Swank J., Rawley G., et al., 1994, AIP Conf.Ser. 313, 159  
 Corcoran M.F., Rawley G.L., Swank J.H., Petre R., 1995, ApJ 445, L121  
 Corcoran M.F., Rawley G.L., Swank J.H., Petre R., Schmitt J.H.M.M., 1996, MPE-Report 263, 25  
 Corcoran M.F., Ishibashi K., Swank J.H., et al., 1997, Nature 390, 587  
 Corcoran M.F., Petre R., Swank J.H., et al., 1998, ApJ 494, 381  
 Corcoran M.F., Fredericks A.C., Petre R., Swank J.H., Drake S.A., Ishibashi K., 2000, ApJ, in press  
 Currie D.G., Dowling D.M., Shaya E.J., et al., 1996, AJ 112, 1115  
 Daminieli A., 1996, ApJ 460, L49  
 Daminieli A., Conti P.S., Lopes D.F., 1997, New Astronomy 2, 107  
 Davidson K., Walborn N.R., Gull T.R., 1982, ApJ 254, L47  
 Davidson K., Humphreys R.M., 1997, ARA&A 35, 1  
 Dufour R.J., Glover T.W., Hester J.J., et al., 1997, in 'Luminous Blue Variables: Massive Stars in Transition', eds. Nota A., Lamers H.J.G.L.M., ASP Conf. Series 120, p. 255  
 Duschl W.J., Hofmann K.-H., Rigaut F., Weigelt G., 1995, RevMexAA SdC 2, 41  
 Forman W., Jones C., Cominsky L., et al., 1978, ApJS 38, 357  
 Gaviola E., 1946, RevAstron 18, 252  
 Gaviola E., 1950, ApJ 111, 408  
 Harris D. E., Silverman J. D., Hasinger G., Lehmann I., 1998, A&AS 133, 431  
 Herschel J.F.W., 1847, Results of Astronomical Observations Made During the Years 1834-1888 at the Cape of Good Hope, London, 32  
 Hill R.W., Burginyon G., Grader R.J., et al., 1972, ApJ 171, 519  
 Hiller D.J., Allen D.A., 1992, A&A 262, 153  
 Humphreys R.M., 1978, ApJS 38, 309  
 Humphreys R.M., 1979, ApJS 39, 389  
 Humphreys R.M., Davidson K., 1979, ApJ 232, 409  
 Humphreys R.M., Davidson K., 1994, PASP 106, 1025  
 Humphreys R.M., Davidson K., Smith N., 1999, PASP 111, 1124  
 Innes R.T.A., 1903, Cape Ann. 9, 75B  
 Koyama K., Ikuko A., Ushimaru N., Yamauchi S., Corbet R.H.D., 1990, ApJ 362, 215  
 Langer N., Hamann W.-R., Lennon M., et al., A&A 290, 819  
 McKee C.F., 1987, in 'Spectroscopy of Astrophysical Plasmas', eds.: Dalgarno A., Layzer D., Cambridge University Press, Cambridge, p.226  
 Meaburn J., Wolstencroft R.D., Walsh J.R., 1987, A&A 181, 333  
 Meaburn J., Walsh J.R., Wolstencroft R.D., 1993, A&A 268, 283  
 Meaburn J., Boumis P., Walsh J.R., et al., 1996, MNRAS 282, 1313  
 Morse J.A., Davidson K., Bally J., et al., 1998, AJ 116, 2443  
 Nota A., Livio M., Clampin M., Schulte-Ladbeck R., 1995, ApJ 448, 788  
 Savage B.D., Bohlin R.C., Drake F.J., Budich W., 1977, ApJ 216, 291  
 Schmutzler T., Tscharnuter W.M., 1993, A&A 273, 318  
 Seward F.D., Chlebowski T., 1982, ApJ 256, 530  
 Seward F.D., Page C.G., Turner M.J.L., Pounds K.A., 1976, MNRAS 177, 13P  
 Seward F.D., Forman W.R., Giacconi R., et al., 1979, ApJ 234, L55  
 Seward F.D., et al., 2001, ApJ, submitted  
 Shull J.M., van Steenburg M., 1982, ApJS 48, 95 and erratum ApJS 49, 351  
 Stahl O., Daminieli A., 1998, in 'Cyclical Variability in stellar winds', proceedings of the ESO workshop, eds.: Kaper L., Fullerton A.W., Springer, p.112  
 Sutherland R.S., Dopita M.A., 1993, ApJS 88, 253  
 Thackeray A.D., 1949, Obs 69, 31  
 Thackeray A.D., 1950, MNRAS 110, 524  
 Tsuboi Y., Koyama K., Sakano M., Petre R., 1997, PASJ 49, 85  
 van Genderen A. M., Thé P.S., 1984, SpaceSciRev 39, 317  
 Viotti R., 1995, RevMexAA SdC 2, 10  
 Walborn N.R., 1976, ApJ 204, L17

Walborn N.R., Blanco B.M., Thackeray A.D., 1978, ApJ 219, 498

Walborn N.R., Blanco B.M., 1988, PASP 100, 797

Weis K., Duschl W.J., Chu Y-H., 1999, A&A 349, 467

Weis K., 2000, in ' $\eta$  Carinae and other mysterious stars', eds.: Gull T., Johanson S., Davidson K., ASP Conf. Series, submitted